RADIO AND X-RAY EMISSION AS PROBES OF TYPE IIP SUPERNOVAE AND RED SUPERGIANT MASS LOSS

Roger A. Chevalier[1], Claes Fransson[2], Tanja K. Nymark[2],

ABSTRACT

Type IIP (plateau) supernovae are thought to come from stars with initial mass $\sim 8-25\ M_\odot$ that end their lives as red supergiants. The expected stellar end points can be found from evolutionary calculations and the corresponding mass loss properties at this point can be estimated from typical values for Galactic stars. The mass loss densities of observed supernovae can be estimated from observations of the thermal X-ray and radio synchrotron emission that result from the interaction of the supernova with the surrounding wind. Type IIP supernovae are expected to have energy-conserving interaction during typical times of observation. Because Type IIP supernovae have an extended period of high optical luminosity, Compton cooling can affect the radio emitting electrons, giving rise to a relatively flat radio light curve in the optically thin regime. Alternatively, a high efficiency of magnetic field production results in synchrotron cooling of the radio emitting electrons. Both the X-ray and radio luminosities are sensitive to the mass loss and initial masses of the progenitor stars, although the turn-on of radio emission is probably the best estimator of circumstellar density. Both the mass loss density and the variation of density with stellar mass are consistent with expectations for the progenitor stars deduced from direct observations of recent supernovae. Current observations are consistent with mass being the only parameter; observations of a supernova in a metal poor region might show how the mass loss depends on metallicity.

Subject headings: stars: circumstellar matter — stars: mass loss — supernovae

1. INTRODUCTION

SNe IIP (Type IIP supernovae) may be relatively straightforward to interpret in terms of stellar evolution models. They are characterized by a long, plateau light curve that

[1]Department of Astronomy, University of Virginia, P.O. Box 3818, Charlottesville, VA 22903; rac5x@virginia.edu

[2]Department of Astronomy, Stockholm University, AlbaNova, SE–106 91 Stockholm, Sweden

can be attributed to the H envelope of the progenitor star. The progenitor stars have not undergone strong mass loss and are consistent with $\sim 8 - 25\ M_{\odot}$ stars that have evolved as single stars (e.g., Heger et al. 2003). Stellar evolution models, models of supernova light curves, and observations of supernova progenitors all suggest that these stars explode as red supergiants.

Although only a fraction of the stellar mass is lost, red supergiants are known to have slow winds that provide a target for the expanding supernova. The properties of these winds, based on empirical fits to stellar observations, are an important input to stellar evolution models. The supernova interaction with the wind generates a hot, shocked region that can be observed by X-ray emission and by radio synchrotron emission from relativistic electrons (Weiler et al. 1986; Chevalier & Fransson 2003). SNe IIP provide an excellent place to study the interaction because asymmetries may not be significant and rapid evolution is not expected before the supernova. The main parameters determining the mass loss and explosion properties are expected to be the mass and metallicity of the progenitor star, although rotation could also play a role.

The expected mass loss rates and hydrodynamic interaction are described in § 2. The resulting radio and X-ray emission properties are discussed in the context of observations of SNe IIP in § 3 and § 4, respectively. The relation of progenitor mass, deduced from the recent identifications of the stellar progenitors of SNe IIP, to mass loss is treated in § 5.

2. HYDRODYNAMIC INTERACTION

Calculations of massive star evolution typically include mass loss by using a parametrized fit to observed stellar mass loss rates. A number of evolutionary calculations (e.g., Schaller et al. 1992; Heger et al. 2003) use the parametrizations of de Jager, Nieuwenhuijzen, & van der Hucht (1988) or Nieuwenhuijzen & de Jager (1990). An older parametrization specifically for cool stars is that of Reimers (1977). Fig. 1 shows the values of $\dot{M}$ at the time of the explosion using the evolutionary tracks of Schaller et al. (1992), including the values given by Schaller et al. based on de Jager, Nieuwenhuijzen, & van der Hucht (1988) and values derived from the expression of Reimers (1977). The uncertainty in the mass loss rates is estimated by the authors to be about a factor of 2, which is comparable to the difference between the two parametrizations. More recent evolutionary tracks, like those given in Smartt et al. (2004), are in close agreement with those given by Schaller et al. (1992). Although the exact mass limits over which SNe IIP occur are not known, it can be seen that $\dot{M}$ varies over about an order of magnitude.

In these models, the progenitor star does not enter a 'superwind' phase at the end of its life. Eldridge & Tout (2004) find that the stellar luminosity can rise at the second dredge-up at the end of a star's life, presumably giving a rise in the mass loss rate, perhaps driven by thermal pulses. The upper initial mass limit for which the dredge-up occurs depends on convective overshoot: 8 $M_\odot$ limit for overshooting and 10 $M_\odot$ limit for no overshooting. If much of the envelope is lost, the supernova may not be of Type IIP. Chugai (1997) has discussed how supernovae with dense wind interaction may have progenitors near the low mass limit.

The above results are for solar metallicity, $Z \approx 0.02$, where Z is the heavy element mass fraction. Evolutionary calculations typically assume that $\dot{M} \propto Z^{0.5}$ (Schaller et al. 1992; Heger et al. 2003), although this dependence does not have a sound basis in either theory or observations of cool stars.

Another possible parameter for mass loss is stellar rotation. Meynet & Maeder (2000) find a significant dependence of the mass loss rates as a function of rotation. If we assume that most of the He-burning takes place in the red supergiant phase (as is true for the rotating models although the nonrotating low mass models spend some time as a blue supergiant) we find $\dot{M} = (0.84{-}1.6){\times}10^{-6}$ $M_\odot$ yr^{-1} for the 15 $M_\odot$ models and $(3.0{-}6.2){\times}10^{-6}$ $M_\odot$ yr^{-1} for the 20 $M_\odot$ models for non-rotating and 300 km s^{-1} rotating models, respectively. Meynet & Maeder argue that the 300 km s^{-1} models are the more realistic. The values for the 300 km s^{-1} rotation models agree with the numbers in Fig. 1, while the non-rotating values are a factor of two lower.

The important mass loss parameter for supernova interaction is the wind density, ρ_w, determined by the parameter A, where $\rho_w = Ar^{-2} = \dot{M}/4\pi v_w r^2$ and v_w is the wind velocity. The wind velocity for a red supergiant is typically $10 - 15$ km s^{-1}. There is not a well-developed theory for the winds from red supergiants, but general considerations of winds typically have v_w proportional to escape velocity, or $v_w \propto M^{1/2}/R^{1/2}$, where R is the stellar radius. For the range of cases shown in Fig. 1, the resulting variation in v_w is $< 10\%$ about a mean value, with the 7 $M_\odot$ star having a high value and the 20 $M_\odot$ star having a low value. The variation in wind density is thus only slightly larger than that in $\dot{M}$ alone.

For the structure of the supernova, we use the results of Matzner & McKee (1999) for the explosion of a red supergiant. These models assume that the outer envelope can be approximated as an $n = 3/2$ polytrope, which is accurate if the convection is efficient. The results for the exploded outer structure depend on q, the fraction of the total progenitor mass that is inside the H envelope. Since we are mainly concerned with stars that have not undergone extensive mass loss, we take $q = 0.3$. We have considered the interaction of the harmonic mean density profile of Matzner & McKee with a stellar wind typical of that

expected around a SN IIP and found that the density over the time of interest ($\sim$ 1 yr) is well approximated by the outer power law density region. The density in this region can be expressed as $\rho_{SN} \propto t^{-3}(r/t)^{-n}$ with $n = 11.73$. For this power law profile, the outer shock wave expands as $R \propto t^{(n-3)/(n-2)} \propto t^{0.90}$. If the wind interaction is considered in the thin shell approximation (Chevalier 1982), the shell velocity is given by

$$V_s = 1.6 \times 10^4 \left(\frac{\dot{M}_{-6}}{v_{w1}}\right)^{-0.10} E_{51}^{0.45} \left(\frac{M_{ej}}{10\ M_\odot}\right)^{-0.345} \left(\frac{t}{10\ \mathrm{day}}\right)^{-0.10} \mathrm{km\ s^{-1}}, \qquad (1)$$

where $\dot{M}_{-6}$ is the wind mass loss rate in units of $10^{-6}\ \ M_\odot\ \mathrm{yr}^{-1}$, v_{w1} is the wind velocity in units of 10 km s^{-1}, E_{51} is the explosion energy in units of 10^{51} ergs, and M_{ej} is the ejecta mass. The temperature of the gas at the reverse shock front is $T_r = 1.2V_{s4}^2$ keV, where V_{s4} is the shell velocity in units of 10^4 km s^{-1}. The model velocities can be compared to observed velocities in SNe IIP deduced from absorption lines, which give a minimum value for the free expansion velocity at the interaction point. Elmhamdi et al. (2003) find a maximum velocity of $\sim 16,000$ km s^{-1} for the blue wing of H-alpha in SN 1999em at an age of 9 days. This velocity is difficult to determine accurately because of blending with other lines; however, the better defined absorption minimum is at $12,500$ km s^{-1}, lending support to the above maximum velocity.

Another consideration for the maximum ejecta velocity is that it may be limited by radiation losses at the time of shock breakout, independent of the circumstellar interaction. For a red supergiant with radius 500 $R_\odot$ and standard supernova parameters, equation (32) of Matzner & McKee (1999) gives a maximum velocity of $\sim 13,000$ km s^{-1}, indicating that this could be a limiting factor.

In the interaction model, the cooling time for gas at the reverse shock is equal to the age at an age

$$t_c \approx 20 \dot{M}_{-6} v_{w1}^{-1} V_{s4}^{-5.2} \mathrm{days}. \qquad (2)$$

Substitution of equation (1) for V_{s4} yields

$$t_c = 0.26 \left(\frac{\dot{M}_{-6}}{v_{w1}}\right)^{3.2} E_{51}^{-4.9} \left(\frac{M_{ej}}{10\ M_\odot}\right)^{3.7} \mathrm{days}, \qquad (3)$$

valid for a reverse shock temperature $\lesssim 2 \times 10^7$ K, or for $n = 11.73$ and $V_s \lesssim 12,000$ km s^{-1} (Chevalier & Fransson 2003). Considering the dependence of $\dot{M}$ on mass (Fig. 1), it can be seen that stars with $M \gtrsim 20\ M_\odot$ have an extended radiative period. However, most SNe IIP are expected to have progenitors of lower mass and to have shocks that are energy conserving except at very early times, before observations typically take place. The presence

of radiative cooling would be expected to give a boxy Hα profile at late times, as seen in SN 1993J (Filippenko, Matheson, & Barth 1994); such a profile has never been reported in a SN IIP.

3. RADIO EMISSION

Radio emission observed from supernovae can be attributed to synchrotron emission from the interaction region between the supernova and the surrounding wind (Chevalier 1982). The mechanisms for particle acceleration and magnetic field amplification are not sufficiently well understood to predict the radio luminosity, L_r. However, with the assumptions that the particle and magnetic energy densities are a constant fraction of the total postshock energy density, we have $L_r \propto (\dot{M}/v_w)^{1.4-2}$ for typical parameters, when the emission is optically thin and at a fixed age (Chevalier 1982). This expression assumes similar supernova properties.

At early times, the radio emission is absorbed; the most likely mechanisms for SNe IIP are FFA (free-free absorption) by ionized gas outside the forward shock front and SSA (synchrotron self-absorption). Optical depth unity to free-free absorption is attained at an age

$$t_{ff} \approx 6 \left(\frac{\dot{M}_{-6}}{v_{w1}}\right)^{2/3} T_{cs5}^{-1/2} V_{s4}^{-1} \left(\frac{\nu}{8.46 \text{ GHz}}\right)^{-2/3} \text{ days}, \quad (4)$$

where T_{cs5} is the circumstellar temperature in units of 10^5 K. The value of T_{cs} is uncertain. Calculations, mainly directed to Type IIL supernovae, by Lundqvist & Fransson (1988) find that for $\dot{M}_{-6}/v_{w1} = 3$ the temperature at the time of optical depth unity was $\sim 3 \times 10^4$ K, while for $\dot{M}_{-6}/v_{w1} = 10$ it was found that $T_{cs} \sim 1 \times 10^5$ K. These calculations used a simplified model for the shock breakout radiation, and may have underestimated the temperature somewhat. In the following we will use $T_{cs} = 1 \times 10^5$ K as a reference value, but we emphasize that this parameter is uncertain.

A number of recent, well-observed SNe IIP are listed in Table 1. The distances to SN 1999em and SN 2004dj are based on Cepheids; for SN 1999em, this distance is 50% larger than the distance determined by the EPM (expanding photosphere method) (Leonard et al. 2003). The EPM distance to SN 1999gi is used; in this case, the Cepheid distances to nearby galaxies are only slightly larger (Leonard et al. 2002). The distance to SN 2002hh and SN 2004et (both in NGC 6946) is based on an average of 3 methods (Li et al. 2005a).

The positions of the SNe IIP, as well as other supernovae, in a peak radio luminosity - time of peak diagram are shown in Fig. 2, which is an update of Fig. 4 of Chevalier (1998).

The times of peak of the SNe IIP were determined from plausible fits to the available data. It can be seen that the SNe IIP cluster in a small region of the diagram. The constant velocity lines in the diagram are based on the assumptions that SSA is the dominant absorption mechanism and that there is energy equipartition between particles and fields (although the results depend only weakly on this assumption). If the velocity deduced in this way is compatible with the maximum velocities in the supernova, SSA is a plausible absorption mechanism. If the velocity is lower than the apparent maximum velocity, another mechanism, such as FFA, must be operating. However, the model assumes that $p = 3$ and that there is no cooling of radio emitting electrons; as shown below, these assumptions are probably not accurate. The position of the SNe IIP, somewhat below the $10,000$ km s^{-1} line, is close to the velocities expected in SNe IIP, indicating that SSA may play a role but other mechanisms, such as FFA, may also be important.

Depending on the parameters characterizing the supernova ejecta, the circumstellar medium, the magnetic field and the relativistic electrons, cooling of the relativistic electrons may be important. As we show below, this has important consequences for both the light curve and the spectrum.

We first consider synchrotron cooling. Assuming that the magnetic field energy density is a fixed fraction ϵ_B of the the thermal energy behind the circumstellar shock, the ratio of the synchrotron time scale to the expansion time scale is given

$$\frac{t_{synch}}{t} \approx 2.0 \left(\frac{\epsilon_B}{0.1}\right)^{-3/4} \left(\frac{\dot{M}_{-6}}{v_{w1}}\right)^{-3/4} \left(\frac{\nu}{10 \text{ GHz}}\right)^{-1/2} \left(\frac{t}{10 \text{ days}}\right)^{1/2}. \quad (5)$$

Therefore, in the restricted range $\dot{M}_{-6}/v_{w1} \gtrsim 4$ and $\epsilon_B \gtrsim 0.1$ synchrotron losses may be important.

Inverse Compton cooling of the relativistic electrons by the strong photon flux from the ejecta can be important especially during the early phases. The ratio of the Compton cooling time scale and expansion time scale is

$$\frac{t_{comp}}{t} \approx 0.18 \left(\frac{L_{\rm bol}}{2 \times 10^{42} \text{ erg s}^{-1}}\right)^{-1} \left(\frac{\epsilon_B}{0.1}\right)^{1/4} \left(\frac{\dot{M}_{-6}}{v_{w1}}\right)^{1/4} V_{s4}^2 \left(\frac{\nu}{10 \text{ GHz}}\right)^{-1/2} \left(\frac{t}{10 \text{ days}}\right)^{1/2}, \quad (6)$$

where $L_{\rm bol}$ is the bolometric luminosity of the supernova. Depending on $L_{\rm bol}, \dot{M}$, and the highly uncertain value of ϵ_B, inverse Compton cooling may or may not be important. In general, low values of ϵ_B and $\dot{M}$ favor inverse Compton cooling.

There are few well determined bolometric light curves of Type IIP supernovae. Observations of the normal Type IIP SN 1992H show that $L_{\rm bol}$ decreased from $\sim 3 \times 10^{42}$ erg s^{-1}

to $\sim 1.3 \times 10^{42}$ erg s^{-1} during the first ~ 50 days, and then stayed constant up to ~ 100 days, when it dropped (Clocchiatti et al. 1996). There is, however, a considerable range in luminosities within the IIP class. Hamuy (2003) finds that the absolute magnitude during the plateau phase varies between $M_V = -15.37$ and $M_V = -18.57$, with $M_V = -17.41$ for SN 1992H. From modeling of SNe IIP, Eastman et al. (1994) find that at day one $L_{\rm bol} \sim 2.5 \times 10^{42}$ erg s^{-1}, and during the plateau phase $L_{\rm bol} \sim (1-2) \times 10^{42}$ erg s^{-1}, in good agreement with SN 1992H. Chieffi et al. (2003) find a similar luminosity for SNe IIP during the first 50 days. The energy and envelope mass of the models are, however, adjusted to fit the observations, and are not calculated from first principles. Adopting a luminosity of $L_{\rm bol} \sim 1 \times 10^{42}$ erg s^{-1}, we find that for $\epsilon_B \lesssim 0.1$ inverse Compton cooling is likely to be important during most of the plateau phase, except for very high mass loss rates or shock velocities.

Because $t_{comp} \propto \epsilon_B^{1/4}$ and $t_{synch} \propto \epsilon_B^{-3/4}$ the Compton timescale is likely to be short in the cases where the synchrotron timescale is long, and vice versa. In Figure 3 we show how the cooling timescales as function of the parameter $\epsilon_B A_* \equiv \epsilon_B \dot{M}_{-5}/v_{w1}$. Because both the synchrotron and Compton cooling timescales are proportional to $(t/\nu)^{0.5}$ we plot the scaled cooling timescale $t_{cool}(t_{10}/\nu_{10})^{0.5}/t$, where $t_{10} = t/10$ days and $\nu_{10} = \nu/10$ GHz. The remaining parameter is then $l_{42} = (L_{\rm bol}/10^{42}$ erg s$^{-1})(V_s/15,000$ km s$^{-1})^{-2}$.

As an example, for $\dot{M}_{-5}/v_{w1} = 1$, $\epsilon_B = 0.1$, $\nu = 10$ GHz, $l_{42} = 1$ and $t = 10$ days we get $t_{\rm comp}/t \approx 1$ and $t_{\rm synch}/t \approx 0.3$. For the same parameters, but with $\epsilon_B = 10^{-3}$, we instead obtain $t_{\rm comp}/t \approx 0.3$ and $t_{\rm synch}/t \approx 10$. In both cases the electrons are cooling, but in the former case by synchrotron cooling and in the latter by Compton cooling.

The fact that cooling is likely to be important in many cases for the relativistic electrons means that the spectral index of the radio emission (flux $\propto \nu^{-\alpha}$) is expected to be steep with $\alpha \approx 1.0$, if the particles are injected with an energy spectral index $p \approx 2$. As cooling becomes less important at late times, the spectrum should flatten toward $\alpha \approx 0.5$. This is one of the important diagnostics of cooling.

To show the possible range of radio light curves, we have calculated radio light curves for four different cases, two where cooling is important, one 'minimal cooling' case, and one purely adiabatic case. All calculations have $p = 2.2$, $\dot{M}_{-6}/v_{w1} = 5$, $n = 11.73$ and $V_s = 15,000$ km s^{-1} at 10 days. For the bolometric light curve we take that of SN 1992H and scale it by a factor $f_{\rm bol}$. For each value of $f_{\rm bol}$ we vary ϵ_B and ϵ_r to give a peak flux of 2 mJy at 4.9 GHz at 5 Mpc, typical of the observed Type IIP light curves. Figure 3 and equations (5) and (6) show that one can have two qualitatively different cases of cooling. For high values of ϵ_r (and therefore small values of ϵ_B) Compton cooling dominates. Conversely, large values of ϵ_B imply synchrotron cooling. We therefore calculate two models typical of

these cases, one, model C, with $f_{\rm bol} = 1$, $\epsilon_B = 0.0013$ and $\epsilon_r = 0.05$, and one, model S, with $f_{\rm bol} = 1$, $\epsilon_B = 0.15$ and $\epsilon_r = 0.001$.

To find parameters relevant for a realistic non-cooling case is non-trivial. To minimize inverse Compton losses, and still be within the range of reasonable bolometric luminosities, we take $f_{\rm bol} = 0.05$ and $V_s = 20,000$ km s^{-1}. During the plateau phase this corresponds to $L_{\rm bol} \sim 1 \times 10^{41}$ erg s^{-1}, giving $l_{42} = 5.6 \times 10^{-2}$. From Figure 3 we see that minimum cooling then occurs for $\epsilon_B \dot{M}_{-5}/v_{w1} \approx 2 \times 10^{-3}$. With $\dot{M}_{-5}/v_{w1} = 1$, to reproduce the approximate turn-on time we require $\epsilon_r \approx 1 \times 10^{-2}$ to give the approximate flux level. We refer to this as model M. Finally for comparison, we show one model, model A, where we have artificially put both synchrotron and inverse Compton cooling to zero. In Figure 4 we show the resulting light curves for 5.0, 8.46, and 22.5 GHz.

The most interesting aspect of these light curves is the variation in the optically thin decline rate. While the flux in the adiabatic model, model A, falls off as $F_\nu \propto t^{-(p+5-6m)/2} = t^{-0.8}$, the others have a flatter evolution. Here $m = (n-3)/(n-2) = 0.9$ for $n = 12$. This is especially true for Model C, which is dominated by Compton cooling of the electrons. Because the Compton cooling rate depends on the bolometric luminosity of the supernova, the radio light curve reflects the shape of the bolometric, primarily optical, light curve. In the limit that $t_{comp} \ll t$ the stationary solution of the kinetic equation for the relativistic electron distribution (Fransson & Björnsson 1998), together with the expression for the synchrotron flux, shows that

$$F_\nu \propto L_{\rm bol}(t)^{-1} t^{m-p/2} \nu^{-p/2}. \quad (7)$$

This shows that the synchrotron flux in this limit is inversely correlated with the bolometric luminosity. Further, for $m \approx 1$ and $p \approx 2$ one obtains a flat light curve in the plateau phase of the bolometric light curve. Note also the dip in the numerical light curves at ~ 100 days, seen especially at the highest frequencies. This coincides roughly with the time when the electrons become adiabatic, which at 5.0 GHz occurs at ~ 80 days for these parameters.

In the synchrotron cooling dominated model S, the cooling has in contrast a smooth evolution, $t_s \propto t^{1/2}$. Consequently, the radio light curve does not show any features like the Compton dominated case. Finally, we note that the minimum cooling case, model M, has a flatter decline than the purely adiabatic case, showing that cooling even for this case cannot be neglected.

The only SNe IIP with sufficient radio data available to compare to our models are SN 2004et and SN 2004dj. In other cases, there are some data on the radio rise, which can be used to estimate the circumstellar density from FFA.

3.1. SN 2004et

The data on SN 2004et, shown in Figure 5, represent the most complete time coverage of any SN IIP. The data are from Stockdale et al. (2004c) before day 20, with additional data at 4.99 GHz after day 20 from Beswick et al. (2004) and Argo et al. (2005). Some additional upper limits at early epochs exist for the 4.99 GHz observations, but these do not add any strong constraints. Because of the good time coverage we have done a more detailed analysis of this supernova than for the other Type IIPs.

The explosion date of SN 2004et is well constrained to be 22.0 September, 2004, within one day (Li et al. 2005a). The light curve of SN 2004et showed that it was a Type IIP supernova, although it showed some differences from typical Type IIP events (Li et al. 2005a). For the simulations below we use the bolometric light curve of SN 1992H, scaled with $f_{\rm bol} = 0.5$. From the spectra of Li et al. (2005a) we find a maximum velocity of $\sim 14,200$ km s^{-1} for the red wing of the Hα line at days 9 and 20. Because of occultation and other effects this is only a lower limit, and in the following we will use an expansion velocity of $15,000$ km s^{-1} at 10 days. The relative turn-on times between the different frequencies depend on the value of n, and we here take $n = 10$. A smaller value may give a better agreement with the observed turn-on times, but would also result in steeper decays in the optically thin parts of the light curves. All models have an injected electron spectrum with $p = 2.2$. Cooling considerably steepens the integrated spectrum.

As discussed above, we vary the value of ϵ_B, and consequently ϵ_r, to cover both a Compton dominated and a synchrotron dominated case. In Figure 5 we show two sets of light curve fits with either large or small values of ϵ_B and ϵ_r, $\epsilon_B = 0.2$ and $\epsilon_r = 0.001$, and $\epsilon_B = 0.0013$ and $\epsilon_r = 0.04$, respectively. The value of $\dot{M}_{-6}/v_{w1}$ is determined by the turn-on time, but, as pointed out before, also depends on the uncertain temperature of the CSM. In the first case we obtain $\dot{M}_{-6}/v_{w1} = 9\ T_{cs5}^{3/4}$, and in the second $\dot{M}_{-6}/v_{w1} = 10\ T_{cs5}^{3/4}$.

The two cases result in fairly similar light curves, both strongly affected by cooling during the first ~ 100 days. The main difference is that for $\lesssim 20$ days the Compton dominated case shows a lower peak flux for the higher frequencies compared to the lower. This is caused by the decreasing Compton cooling rate with time, which affects the higher frequencies, which first become optically thin and also have a higher Lorentz factor of the electrons. In addition, as we have already found, at later epochs the light curves are flatter than for the synchrotron dominated case. The considerable error bars of the observations, especially at early time, make it difficult to favor one of these cases over the other. Because of the difference in decay slope it is of great interest to pursue these observations to as late times as possible to check these alternatives. The frequency dependent dip in the light curve at ~ 100 days in the Compton case would be an interesting signature. However, effects connected with a

gas density gradient different from a simple $\rho \propto r^{-2}$ wind may also influence the late time behavior and high observational accuracy would be required to detect the dip.

In the $\epsilon_B = 0.0013$, $\epsilon_r = 0.04$ model, the optical depths to synchrotron self-absorption and free-free absorption are similar, while in the $\epsilon_B = 0.2$, $\epsilon_r = 0.001$ model the SSA optical depth is larger than 1 when it becomes thin to FFA. Therefore, especially in the latter model the light curve and spectrum are affected by SSA, giving a slower, more gradual rise compared to pure FFA.

3.2. SN 2004dj

A spectrum of SN 2004dj at the beginning of August 2004 indicated a normal Type IIP supernova (very similar to SN 1999em) with an age of about 3 weeks (Patat et al. 2004). We take 1 August, 2004 to correspond to an age of 21 days. The radio data in this case include a point at 8.4 GHz (Stockdale et al. 2004a), two at 1.4 GHz (Chandra & Ray 2004), and more extensive coverage at 4.99 GHz (Beswick et al. 2005).

As in the case of SN 2004et, there is no single unique combination of ϵ_B and ϵ_r that fits the observations. In Fig. 6 we show two examples, one with small ϵ_B and large ϵ_r, and one for which the opposite is the case. The mass loss rate parameter is rather well constrained by the rising 1.4 GHz points, due to decreasing absorption. The observed sharp rise between days 33 and 43 is suggestive of FFA, although SSA cannot be ruled out. In fact, the $\epsilon_B = 0.01$, $\epsilon_r = 0.0009$ model is dominated by SSA, while FFA is dominant for the $\epsilon_B = 0.00075$, $\epsilon_r = 0.01$ model. We find that $\dot{M}_{-6}/v_{w1} = 2 - 3\ T_{cs5}^{3/4}$ for the two models.

3.3. SN 2002hh

Radio data on SN 2002hh are available from Stockdale et al. (2004b) and Chandra, Ray, & Bhatnagar (2003) for data at 1.4 GHz. The supernova was discovered on 31.1 October, 2002 and a spectrum on 2 November, 2002 showed that it was a very young, highly reddened Type II supernova (Filippenko, Foley, & Swift 2002). We take the age at the time of discovery to be 2 days. There are no published optical light curve observations, as yet, that identify SN 2002hh as a plateau type. However, optical spectra of the supernova in the nebular phase show that it has slow moving H (Mattila et al. 2004); the mixing of H to low velocities is expected to require a massive H envelope compared to the core, as occurs in a SN IIP. Also, its radio properties are similar to other SNe IIP.

The radio rise suggests optical depth unity to FFA at 1.4 GHz on day 62. Table 2 lists

the resulting value of $\dot{M}_{-6} v_{w1}^{-1} T_{cs5}^{-3/4}$. This quantity is $\propto V_{s4}^{3/2}$; the value $V_{s4} = 1.5$ at 10 days has been taken and allowed to evolve $V_{s4} \propto t^{-0.1}$. At the relatively low circumstellar density for SN 2002hh and other SNe IIP, Compton heating to $\sim 5 \times 10^4 - 10^5$ K occurs and recombination is not important (see above, Lundqvist & Fransson 1988).

A different picture for the circumstellar medium of SN 2002hh comes from its infrared detection which Barlow et al. (2005) find is due to dust in circumstellar mass loss $\sim 5 \times 10^{17}$ cm from the supernova based on the infrared spectrum and luminosity. A similar radius for the dust can be obtained by considering that the duration of the infrared emission should be comparable to the light travel time across the emitting region and the total radiated energy should be approximately that radiated optically by the supernova. Barlow et al. (2005) estimate the dust mass to be $0.10 - 0.15\ M_\odot$, corresponding to a gas mass of $10 - 15\ M_\odot$, and attribute a significant part of the $A_V \approx 5$ extinction toward the supernova to this dust. Supernova dust echoes were first inferred around SN 1979C and SN 1980K for which Dwek (1983) found circumstellar optical depths of 0.3 and 0.03 respectively. Scaling with mass loss density and using our value of $\dot{M}/v_w$ leads to an optical depth $\lesssim 0.01$ for SN 2002hh, which would not contribute a significant extinction. An estimate of the mass loss rate from the mass and size of the dust emitting region also leads to a rate $\sim 10^2$ times larger than that estimated from the radio emission.

In principle, there is no contradiction between these observations; the radio emission samples a region inside of the dust emitting region. There may be a rise in the radio emission in $15-20$ years. However, the evidence for the loss of $10-15\ M_\odot$ of gas is difficult to reconcile with the slow moving H in the supernova, which would seem to require a massive H envelope at the time of the explosion.

3.4. Other Supernovae

SN 1999em was a well-observed, normal Type IIP supernova, including evidence for slow H in the nebular phase (Elmhamdi et al. 2003). The radio and X-ray data on it have already been discussed in terms of circumstellar interaction by Pooley et al. (2002). The peak in the light curve is suggested by the comparable fluxes at 1.4 and 4.9 GHz at days $50 - 70$ (see Fig. 2 of Pooley et al. 2002). If not for these, the data could only give an upper limit for the time of peak flux. However, the agreement of the results here with those from the other supernovae suggests that the flux peak was observed. An estimate of the mass loss rate is given in Table 2.

The low luminosities of the detected SNe IIP show that the published upper limits that

have been set for radio supernovae (e.g., Weiler et al. 1989; Eck, Cowan, Branch 2002) are above the expected flux levels for supernovae of this type. However, an upper limit of 0.07 mJy (8.46 GHz) for SN 2003gd on 17 June, 2003 (Stockdale 2003) is more stringent. The age of the SN IIP was ~ 87 days at that time (Van Dyk, Li, & Filippenko 2003). Assuming models similar to those discussed above, the limit is consistent with the expected flux of SN 2004dj, but is a factor ~ 3 lower than the expected fluxes of SNe 2002hh and 2004et. These results suggest an upper limit $\dot{M}_{-6}/v_{w1} \lesssim 3$.

4. X-RAY EMISSION

We first consider the thermal emission from the shocked region. The monochromatic luminosity of the circumstellar shock can be estimated from

$$\frac{dL_{\rm cs}}{dE} \approx 6.9{\times}10^{35}\zeta T_9^{-0.08} E_{\rm keV}^{-0.23} e^{-0.0116E_{\rm keV}/T_9} \left(\frac{\dot{M}_{-6}}{v_{w1}}\right)^2 V_{s4}^{-1} \left(\frac{f}{0.2}\right)^{-1} \left(\frac{t}{10\ {\rm days}}\right)^{-1} \ {\rm ergs\ s^{-1}\ keV^{-1}} \tag{8}$$

(Nymark, Fransson, & Kozma 2005). Here $T_9 = T_{\rm e}/10^9$ K, $E_{\rm keV}$ is the photon energy in keV, f is the relative thickness of the circumstellar shock region, and $\zeta = [1 + 2n({\rm He})/n({\rm H})]/[1 + 4n({\rm He})/n({\rm H})] \approx 0.86$ for solar composition. For $n = 7$ we have $f \approx 0.3$, and for $n \gtrsim 12$, $f \approx 0.22$ (Chevalier & Fransson 1994). The electron temperature, $T_{\rm e}$, is uncertain because of the unknown importance of collisionless heating. If only Coulomb collisions are important $5 \times 10^8 \lesssim T_{\rm e} \lesssim 1 \times 10^9$ K. The luminosity from equation (8) should be added to the flux from the reverse shock below.

If the reverse shock is in the nonradiative regime and free-free emission dominates, which is a good approximation for $T \gtrsim 5 \times 10^7$ K, the X-ray luminosity at ~ 1 keV is given by (Fransson, Lundqvist, & Chevalier 1996)

$$\frac{dL_{\rm rev}}{dE} = 2.0{\times}10^{35}\zeta(n{-}3)(n{-}4)^2 T_8^{-0.024} e^{-0.116/T_8} \left(\frac{\dot{M}_{-6}}{v_{w1}}\right)^2 V_{s4}^{-1} \left(\frac{t}{10\ {\rm days}}\right)^{-1} \ {\rm ergs\ s^{-1}\ keV^{-1}}. \tag{9}$$

The main variation of X-ray luminosity with wind density is the $(\dot{M}_{-6}/v_{w1})^2$ term. Both equations (8) and (9) assume that the ingoing half of the X-ray emission is absorbed by the ejecta. In general, the emission from the reverse shock dominates in the keV region, unless the shock is radiative so that absorption by the cool dense shell is important.

For $T \lesssim 5 \times 10^7$ K, line emission becomes important and a more detailed calculation of the spectrum of the reverse shock is required. For this we have used the code described in Nymark, Fransson, & Kozma (2005) which calculates the ionization and emission for a

given electron temperature and density. Because the reverse shock, for the mass loss rates discussed here, is nonradiative, we assume that the ion temperature and density are given by the self-similar structure for the particular value of n. The electron temperature is calculated assuming Coulomb collisions only. For the reverse shock, this is enough to bring electrons and ions into equipartition. The ionization is calculated from the time a given element is shocked to the observed epoch, using the full time dependent equations. Because only a fraction of the hydrogen envelope has been lost for the Type IIP supernovae, we assume solar composition.

In Fig. 7 we show the resulting X-ray spectra for $n = 7$ and 12, and $V_s = 10,000$ km s^{-1} and $V_s = 15,000$ km s^{-1}. The mass loss rate is assumed to be 5×10^{-6} $M_\odot$ yr^{-1} (for $v_w = 10$ km s^{-1}). Because $dL/dE \propto (\dot{M}_{-6}/v_{w1})^2$ as long as cooling is not important, the spectra can be scaled to other mass loss rates, using this relation. The most interesting thing to note from Fig. 7 is the increasing importance of line emission as the reverse shock temperature decreases. For the models shown, $T_{\rm rev} = 8.5 \times 10^7$ K for $n = 7$, $V_s = 10,000$ km s^{-1}; $T_{\rm rev} = 1.9 \times 10^8$ K for $n = 7$, $V_s = 15,000$ km s^{-1}; $T_{\rm rev} = 1.7 \times 10^7$ K for $n = 12$, $V_s = 10,000$ km s^{-1}; and $T_{\rm rev} = 3.8 \times 10^7$ K for $n = 12$, $V_s = 15,000$ km s^{-1}. While the line complex at ~ 1 keV is especially strong in the $n = 12$ models, it is absent in the $n = 7$ models, where the only lines present are the Fe K lines at ~ 7 keV. The feature at ~ 1 keV is due to Fe XXI–XXIV, O VIII, and Ne IX–X, in this order.

In Fig. 7 we have not included any absorption by the cooling gas behind the reverse shock, the circumstellar medium, or interstellar gas. The first two of these depend on the mass loss rate assumed. The total column density behind the reverse shock is

$$N_{\rm rev} \approx 1.0 \times 10^{21} (n-4) \left(\frac{\dot{M}_{-6}}{v_{\rm w1}}\right) V_{s4}^{-1} \left(\frac{t}{10 \text{ days}}\right)^{-1} \text{ cm}^{-2}. \quad (10)$$

In the case that the gas is cooling (i.e. for $\dot{M}_{-6} \gtrsim 5$ and for early epochs, see eq. [3]) the emission from the reverse shock will be absorbed below $\sim 1.2 (N_{\rm rev}/10^{22} {\rm cm}^{-2})^{3/8}$ keV. Even if the gas is not cooling and $T_{\rm rev} \lesssim 2 \times 10^7$ K, incompletely ionized atoms like Mg, Si, and Fe may in principle contribute to absorption *above* ~ 2 keV (e.g., Krolik & Kallman 1984). However, the opacity at 2 keV is only $\sim 2.5 \times 10^{-24}$ cm^2 for $\sim 10^7$ K, and absorption is unlikely to be important for reasonable parameters unless the gas is cooling.

Both equation (9) and Fig. 7 show that the luminosity is sensitive to n. We found from the models for the radio emission for SNe IIP that $n \gtrsim 12$ is indicated (§ 3). However, for the best observed X-ray SN IIP SN 1999em, Pooley et al. (2002) suggested $n = 7 - 9$ based on studies of the optical spectrum and the moderately high temperature ($kT = 5$ keV) found from the X-ray spectrum. The result was $\dot{M}_{-6}/v_{w1} = 1 - 2$; a higher value of n would lower

the mass loss density, bringing it further from agreement with the value deduced from the radio observations (Table 2).

X-rays may also be produced by inverse Compton emission. As we have seen in § 3, inverse Compton cooling by the photospheric photons may be important. These photons are up-scattered to $\sim 3.1\gamma^2(T_{\rm eff}/10^4{\rm K})$ eV, where γ is the Lorentz factor of the relativistic electrons and $T_{\rm eff}$ the effective temperature of the photospheric emission (Felten & Morrison 1966). Using the expression for the inverse Compton emissivity in Felten & Morrison (1966), one can find the X-ray luminosity, which for the interesting case $p = 3$ (cooling important) takes a simple form,

$$\frac{dL_{\rm IC}}{dE} \approx 8.8 \times 10^{38}\ \epsilon_r \gamma_{\rm min} E_{\rm keV}^{-1}\ \left(\frac{\dot{M}_{-6}}{v_{\rm w1}}\right) V_{s4} \left(\frac{L_{\rm bol}(t)}{10^{42}\ {\rm erg\ s^{-1}}}\right) \left(\frac{t}{10\ {\rm days}}\right)^{-1}\ \ {\rm ergs\ s^{-1}\ keV^{-1}}. \tag{11}$$

Here $\gamma_{\rm min}$ is the minimum Lorentz factor of the relativistic electrons. For other values of p, $dL_{\rm IC}/dE \propto E^{-(p-1)/2}$. The distinguishing property is the power law form, which is the same as that of the optically thin radio spectrum, and the correlation of the time evolution with that of the bolometric luminosity. It is unaffected by any absorption by cool gas behind the reverse shock. An observation of an inverse Compton component would allow a determination of the important parameter $\epsilon_r\gamma_{\rm min}$, and then from the radio observations ϵ_B. The stronger dependence of thermal emission on the circumstellar density implies that thermal emission is relatively more important at high $\dot{M}/v_w$ and inverse Compton at low $\dot{M}/v_w$. At high mass loss rates, when reverse shock cooling becomes important, the inverse Compton component may again dominate, especially at early epochs.

The observed X-ray luminosities are given in Table 1. The data are all from *Chandra* and refer to an age of ~ 30 days. SN 2004dj has an X-ray luminosity slightly higher that SN 1999em and a radio luminosity that is slightly lower (Table 1). This suggests that they have comparable wind densities. Both the radio turn-on and the X-ray luminosity of SN 2002hh indicate that the circumstellar density is somewhat larger in this case. The low X-ray luminosity of SN 1999gi suggests a smaller density in this case (by a factor ~ 3), if the supernova properties are similar to the other cases.

Because of the comparatively low fluxes, the spectral information from the observed supernovae is limited. A detailed comparison with the model spectra, or even a discrimination between thermal and non-thermal spectra, is therefore not possible. Our calculations do, however, show that deeper observations of nearby SNe IIP can give very important constraints on both the mass loss and the shock physics.

5. PROGENITOR MASS AND MASS LOSS

Progenitor mass estimates are from observations of the region of the supernova before the supernova occurred. Studies of this kind have been possible for a number of nearby SNe IIP (see Table 1). In the cases of SN 2003gd and SN 2004et (Li et al. 2005a), progenitor stars have been tentatively identified and, in the case of SN 2004dj, a mass was determined from the properties of a tight cluster at the position of the supernova (Maíz-Apellániz et al. 2005). Both SN 2004dj and SN 2004et are estimated to have progenitor masses $\sim 15\ M_\odot$ for which standard mass loss prescriptions give $\dot{M}_{-6} = 1.5 - 3$; the range is increased to $1 - 7$ when the mass uncertainty for SN2004et is included. The mass loss rate deduced from radio observations of SN 2004dj is consistent with expectations, while that for SN 2004et suggests a mass $\sim 20\ M_\odot$. However, for SN 2004et Li et al. (2005a) find that their tentative progenitor is a yellow, rather than red, supergiant and may have some similarity to the peculiar SN 1987A and SN 1993J, although less extreme. These supernovae had very different radio properties from the normal SNe IIP (see Fig. 2), which have properties close to those of SN 2004et.

If the progenitor mass of SN 2003gd was $8 - 9\ M_\odot$, the mass loss density was a factor of ~ 3 lower than for a $15\ M_\odot$ star (Fig. 1), leading to a radio luminosity $5 - 10$ times smaller at the same age. This is consistent with the upper limit on the radio luminosity and shows the difficulty of observing low mass SNe IIP at radio wavelengths. The observations must be undertaken at an early time and with high sensitivity. The recent Type IIP SN 2005cs in M51 is also estimated to have a relatively low mass progenitor, $8 \pm 1\ M_\odot$ (Li et al. 2005b) or $9^{+3}_{-2}\ M_\odot$ (Maund, Smartt, & Danziger 2005). It has not been reported as an X-ray or radio source.

The initial mass deduced for SN 1999em by Smartt et al. (2003) of $< 15\ M_\odot$ is lower than that found for SN 2004dj by Maíz-Apellániz et al. (2005), but Leonard et al. (2003) found a mass $< 20\ M_\odot$ for SN 1999em. The value of $\dot{M}_{-6}/v_{w1}$ (Table 2) is comparable to that for the other SNe IIP and is consistent with stellar evolution and typical red supergiant mass loss rates for a $15\ M_\odot$ initial mass star.

SN 1999gi was considerably less luminous in X-rays than SN 1999em (Table 1), implying a lower value of $\dot{M}_{-6}/v_{w1}$ by a factor ~ 3 for comparable supernova properties. Considering the relation between M and $\dot{M}$ shown in Fig. 1, a drop in $\dot{M}$ by a factor 3 corresponds to going from a $15\ M_\odot$ initial mass star to an $8\ M_\odot$ initial mass star. This is consistent with the limit $< 12\ M_\odot$ deduced for the progenitor of SN 1999gi.

An independent way to estimate the mass of an exploded star is from the properties of the supernova. From analyses of the light curves of the supernovae, ejecta masses for SN

1999em have been estimated as 15.0 $M_\odot$ (Nadyozhin 2003, for $d = 11.1$ Mpc), 27^{+14}_{-8} $M_\odot$ (Hamuy 2003, for $d = 10.7$ Mpc) and, for SN 1999gi, 18.7 $M_\odot$ (Nadyozhin 2003, for $d = 11.8$ Mpc), 43^{+24}_{-14} $M_\odot$ (Hamuy 2003, for $d = 9.0$ Mpc). With this method, the mass estimate decreases as the distance estimate increases. To obtain the initial mass, the mass of any compact remnant and mass lost during the evolution must be added to the ejecta mass. It can be seen that the masses obtained in this way are larger than the masses obtained from the mass loss or from the direct progenitor observations, although Nadyozhin's value for SN 1999em is fairly close to the value deduced by these other methods. The method is, however, sensitive to several factors. In particular, hydrodynamic mixing, as was found to be very important for the light curve of SN 1987A, may change the mass estimates considerably (e.g., Chieffi et al. 2003). More complex supernova models, including models of the spectra, are needed to see whether better agreement can be found between these methods. The current work makes specific predictions for SN 1999em and SN 1999gi, which have only upper limits from the direct progenitor observations.

Table 1 includes estimates of the metallicity of the regions in which the supernovae occurred. The metallicities are either solar or within a factor of 2 of solar; this variation is expected to have a minor effect on the present discussion if the estimated $Z^{1/2}$ dependence of mass loss is correct. If SNe IIP are discovered in highly metal poor regions, there is the possibility of investigating the metallicity dependence of mass loss.

As the sample of supernovae grows, it will be possible to compare the distribution of observed progenitor masses with that expected for a standard initial mass function. If we consider two mass groups, $8-13$ $M_\odot$ and $13-18$ $M_\odot$, 4 of the 7 supernovae mentioned here (SNe 1999em, 2002hh, 2004dj, and 2004et) belong to the high mass group and 3 (SNe 1999gi, 2003gd, and SN 2005cs) belong to the low mass group. For a Salpeter mass function, there would be a factor 1.7 fewer supernovae in the high mass group compared to the low mass group. At least part of the reason for the observed relative paucity of low mass progenitors may be that they give rise to subluminous supernovae. SN 2005cs had a peak absolute V magnitude of -15.6 (Li et al. 2005b), which is subluminous (see § 3). Also, it is possible that not all stars in the $8-13$ $M_\odot$ range end their lives as SNe IIP. The lower mass cut for supernovae is not well-determined, and stars in this mass range may end their lives as a type of supernova other than a IIP.

In summary, data on the wind interaction and progenitor stars of a small number of SNe IIP are consistent with mass loss estimates and tracks in evolutionary models of $\sim 8-20$ $M_\odot$ single stars. The radio and X-ray emission from SNe IIP is relatively faint, but this emission may provide a check on the mass of the supernova progenitor. In addition, the fact that the radio emitting electrons are likely to be subject to energy loss affects the radio light curves

and gives constraints on the physical properties of the shock interaction. X-ray emission gives additional diagnostics and will be most useful if well-determined spectra can be obtained.

We are grateful to Megan Argo, Rob Beswick, Chris Stockdale, Kurt Weiler, and their collaborators for making radio data available in advance of full publication. This research was supported in part by NSF grant AST-0307366, Chandra grant TM4-5003X, and the Swedish Research Council and National Space Board.

Table 1. Type IIP supernovae

SN	Distance (Mpc)	Metallicity ($Z/Z_\odot$)	L_x(0.5-8 keV) (ergs s^{-1})	Progenitor mass ($M_\odot$)	Refs.
1999em	11.7 ± 1.0	$1 - 2$	9×10^{37}	< 15	1,2,3
1999gi	11.1	~ 2	1.6×10^{37}	< 12	2,4,5
2002hh	5.5 ± 1.0		4×10^{38}	–	6,7
2003gd	9	~ 0.5	–	$8 - 9$	8,9
2004dj	3.2	1	1.5×10^{38}	$15, \sim 12$	10,11,12
2004et	5.5 ± 1.0		–	15^{+5}_{-2}	6

References: (1) Leonard et al. 2003; (2) Smartt et al. 2003; (3) Pooley et al. 2002; (4) Leonard et al. 2002; (5) Schlegel 2001; (6) Li et al. 2005; (7) Pooley & Lewin 2002; (8) Van Dyk et al. 2003; (9) Smartt et al. 2004; (10) Maíz-Apellániz et al. 2004; (11) Wang et al. 2005; (12) Pooley & Lewin 2004.

Table 2. Results for radio supernovae

SN	$t(\tau_{ff} = 1)$ at 1.4 GHz (day)	$\dot{M}_{-6} v_{w1}^{-1} T_{cs5}^{-3/4}$
1999em	52	5
2002hh	62	7
2004dj		$2 - 3$
2004et		$9 - 10$

REFERENCES

Argo, M., Beswick, R., Muxlow, T., Pedlar, A., Fenech, D., & Thrall, H. 2005, (astro-ph/0505487)

Barlow, M. J., et al. 2005, ApJ, 627, L113

Beswick, R. J., Muxlow, T. W. B., Argo, M. K., Pedlar, A., & Marcaide, J. M. 2004, IAU Circ. 8435

Beswick, R. J., Muxlow, T. W. B., Argo, M. K., Pedlar, A., Marcaide, J. M., & Wills, K. A. 2005, ApJ, 623, L21

Chandra, P., Ray, A., & Bhatnagar, S. 2003, IAU Circ. 8041

Chandra, P., & Ray, A. 2004, IAU Circ. 8397

Chevalier, R. A. 1982, ApJ, 259, 302

Chevalier, R. A. 1998, ApJ, 499, 810

Chevalier, R. A., & Fransson, C. 1994, ApJ, 420, 268

Chevalier, R. A., & Fransson, C. 2003, in Supernovae and Gamma-Ray Bursts, ed. K. W. Weiler (Berlin: Springer), 171

Chieffi, A., Domínguez, I., Höflich, P., Limongi, M., & Straniero, O. 2003, MNRAS, 345, 111

Chugai, N. N. 1997, Astronomy Reports, 41, 672

Clocchiatti, A., et al. 1996, AJ, 111, 1286

de Jager, C., Nieuwenhuijzen, H., & van der Hucht, K. A. 1988, A&AS, 72, 259

Dwek, E. 1983, ApJ, 274, 175

Eastman, R. G., Woosley, S. E., Weaver, T. A., & Pinto, P. A. 1994, ApJ, 430, 300

Eck, C. R., Cowan, J. J., & Branch, D. 2002, ApJ, 573, 323

Eldridge, J. J., & Tout, C. A. 2004, MNRAS, 353, 87

Elmhamdi, A., et al. 2003, MNRAS, 338, 939

Felten, J. E., & Morrison, P. 1966, ApJ, 146, 686

Filippenko, A. V., Matheson, T., & Barth, A. J. 1994, ApJ, 108, 2220

Filippenko, A. V., Foley, R. J., & Swift, B. 2002, IAU Circ. 8007

Fransson, C., & Björnsson, C. 1998, ApJ, 509, 861

Fransson, C., Lundqvist, P., & Chevalier, R. A. 1996, ApJ, 461, 993

Hamuy, M. 2003, ApJ, 582, 905

Heger, A., Fryer, C. L., Woosley, S. E., Langer, N., & Hartmann, D. H. 2003, ApJ, 591, 288

Krolik, J. H., & Kallman, T. R. 1984, ApJ, 286, 366

Leonard, D. C., Kanbur, S. M., Ngeow, C. C., & Tanvir, N. R. 2003, ApJ, 594, 247

Leonard, D. C., et al. 2002, AJ, 124, 2490

Li, W., Van Dyk, S. D., Filippenko, A. V., & Cuillandre, J. 2005a, PASP, 117, 121

Li, W., Van Dyk, S. D., Filippenko, A. V., Cuillandre, J. Jha, S., Bloom, J. S., Riess, A. G., & Livio, M. 2005b, ApJ, submitted (astro-ph/0507394)

Lundqvist, P., & Fransson, C. 1988, A&A, 192, 221

Maíz-Apellániz, J., Bond, H. E., Siegel, M. H., Lipkin, Y., Maoz, D., Ofek, E. O., & Poznanski, D. 2005, ApJ, 615, L113

Mattila, S., Meikle, W. P. S., & Greimel, R. 2004, New Astronomy Review, 48, 595

Matzner, C. D., & McKee, C. F. 1999, ApJ, 510, 379

Maund, J. R., Smartt, S. J., & Danziger, I. J. 2005, MNRAS, submitted (astro-ph/0507502)

Meynet, G., & Maeder, A. 2000, A&A, 361, 101

Nadyozhin, D. K. 2003, MNRAS, 346, 97

Nieuwenhuijzen, H., & de Jager, C. 1990, A&A, 231, 134

Nymark, T.K., Fransson, C., & Kozma, C. 2005, submitted to A&A

Patat, F., Benetti, S., Pastorello, A., Filippenko, A. V., & Aceituno, J. 2004, IAU Circ. 8378

Pooley, D., & Lewin, W. H. G. 2002, IAU Circ. 8024

Pooley, D., & Lewin, W. H. G. 2004, IAU Circ. 8390

Pooley, D. et al. 2002, ApJ, 572, 932

Reimers, D. 1977, A&A, 61, 217

Schaller, G., Schaerer, D., Meynet, G., & Maeder, A. 1992, A&AS, 96, 269

Schlegel, E. M. 2001, ApJ, 556, L25

Smartt, S. J., Maund, J. R., Gilmore, G. F., Tout, C. A., Kilkenny, D., & Benetti, S. 2003, MNRAS, 343, 735

Smartt, S. J., Maund, J. R., Hendry, M. A., Tout, C. A., Gilmore, G. F., Mattila, S., & Benn, C. R. 2004, Science, 303, 499

Stockdale, C. J. 2003, priv. comm.

Stockdale, C. J., Sramek, R. A., Weiler, K. W., Van Dyk, S. D., Panagia, N., Pooley, D., & Lewin, W. H. G. 2004a, IAU Circ. 8379

Stockdale, C. J., Sramek, R. A., Rupen, M., Weiler, K. W., Van Dyk, S. D., & Panagia, N. 2004b, http://rsd-www.nrl.navy.mil/7213/weiler/kwdata/02hhdata.asc

Stockdale, C. J., Kaster, B., Weiler, K. W., Van Dyk, S. D., Sramek, R. A., & Panagia, N. 2004c, http://rsd-www.nrl.navy.mil/7213/weiler/kwdata/04etdata.asc

Van Dyk, S. D., Li, W., & Filippenko, A. V. 2003, PASP, 115, 1289

Wang, X., Yang, Y., Zhang, T., Ma, J., Zhou, X., Li, W., Lou, Y.-Q., & Li, Z. 2005, ApJ, 626, L89

Weiler, K. W., Sramek, R. A., Panagia, N., van der Hulst, J. M., & Salvati, M. 1986, ApJ, 301, 790

Weiler, K. W., Panagia, N., Sramek, R. A., van der Hulst, J. M., Roberts, M. S., & Nguyen, L. 1989, ApJ, 336, 421

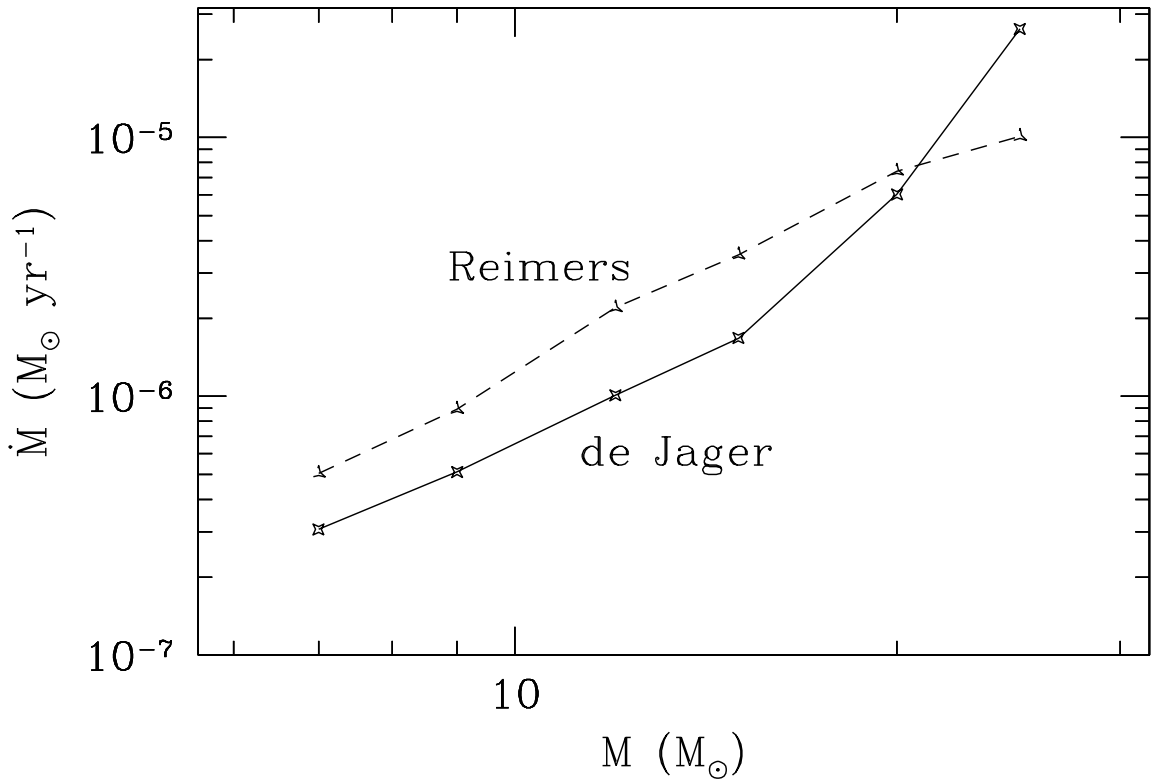

Fig. 1.— Mass loss rates from red supergiants at the end of their lives as a function of initial mass. The stellar endpoints are from $M = 7, 9, 12, 15, 20, 25\ M_\odot$ evolutionary tracks by Schaller et al. (1992), and the mass loss rates are based on de Jager et al (1988) (*solid*) and Reimers (1977) (*dashed*).

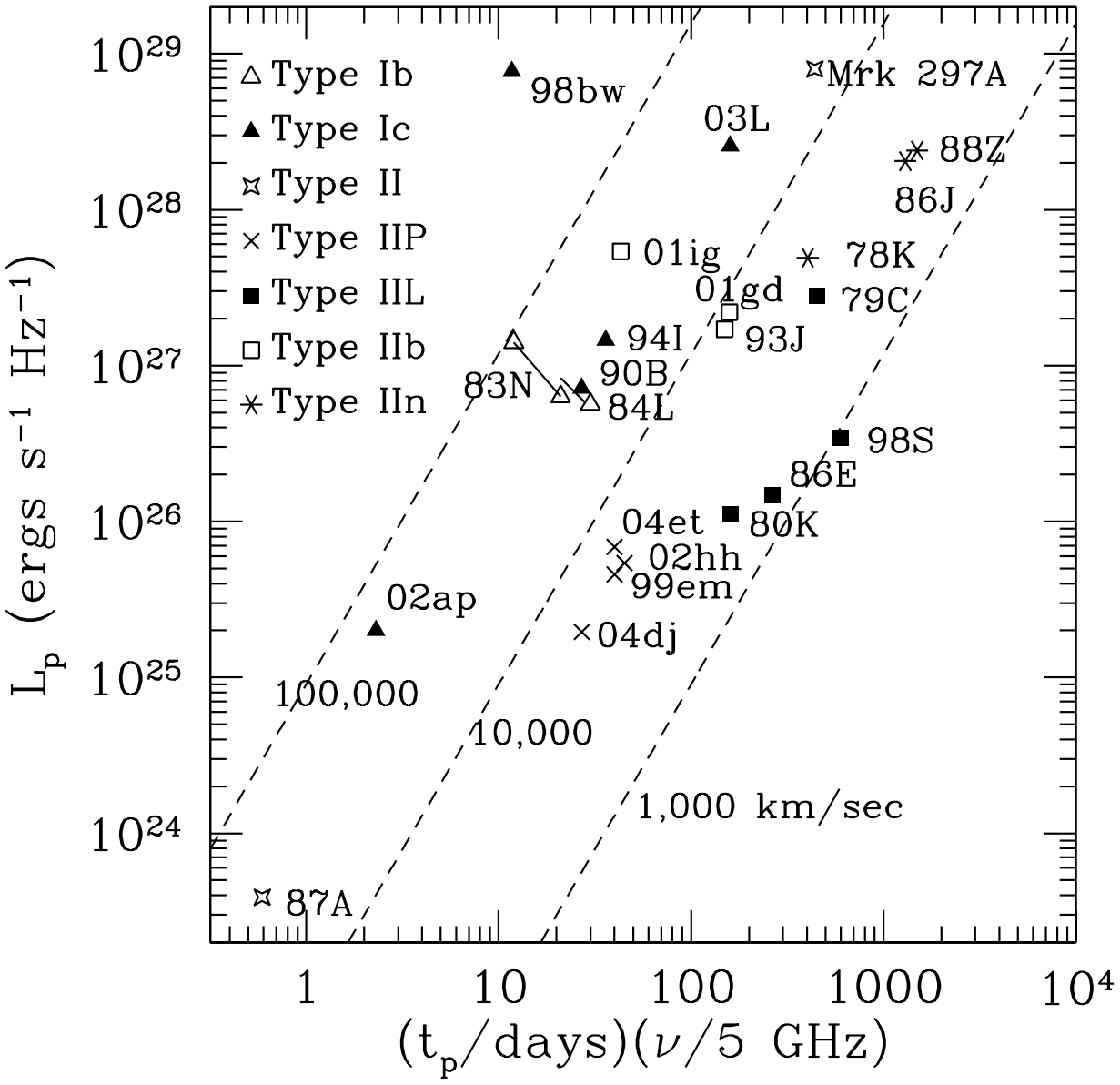

Fig. 2.— Peak radio luminosity vs. time of peak for radio supernovae. The 4 Type IIP supernovae (*crosses*) are near the middle of the plot.

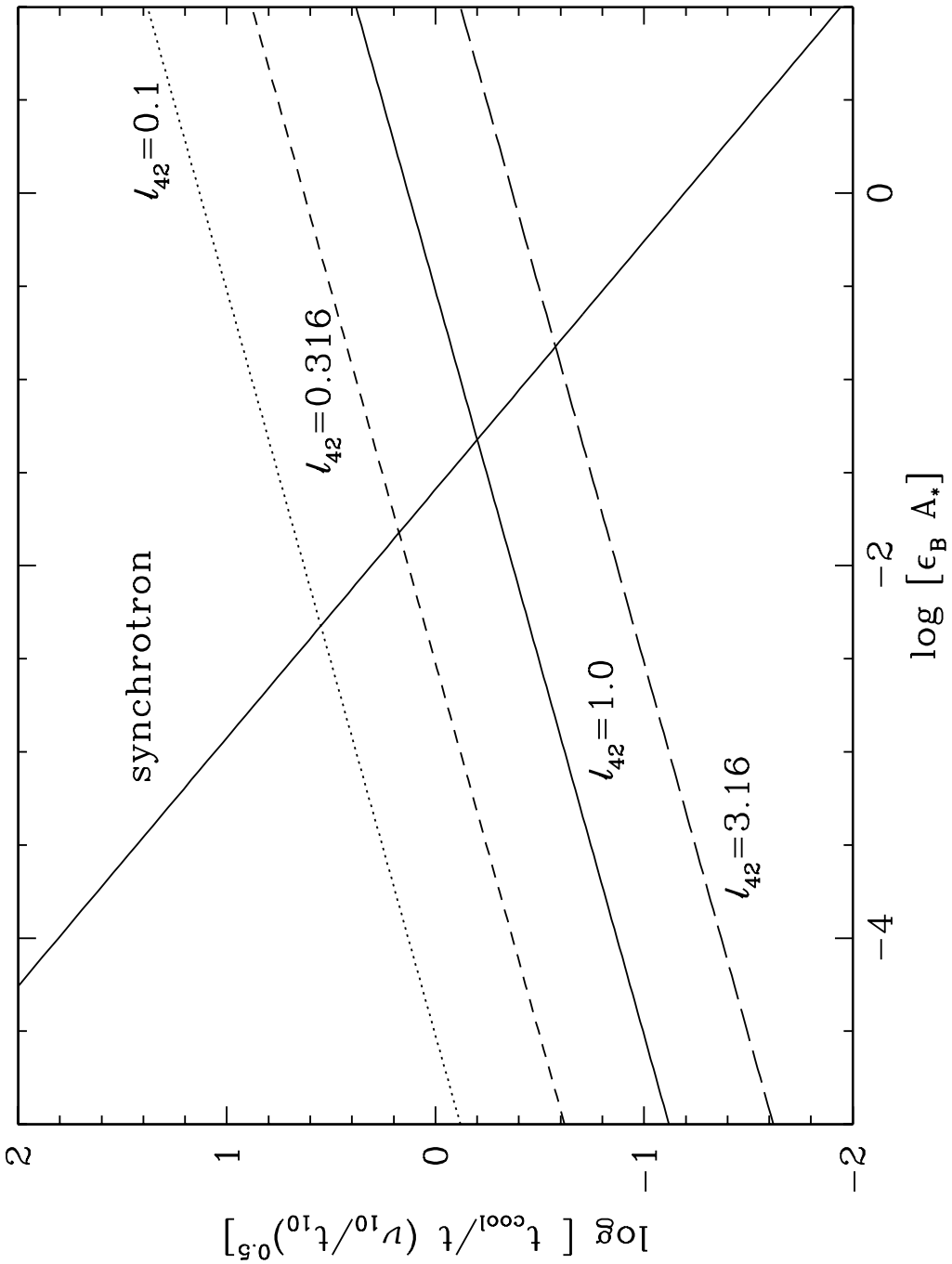

Fig. 3.— Ratio of cooling time scale to adiabatic time scale for synchrotron cooling (single solid line) and for inverse Compton cooling (4 parallel lines). For Compton cooling each curve is labeled with the value of $l_{42} = (L_{\rm bol}/10^{42}$ erg s$^{-1})(V_s/15,000$ km s$^{-1})^{-2}$.

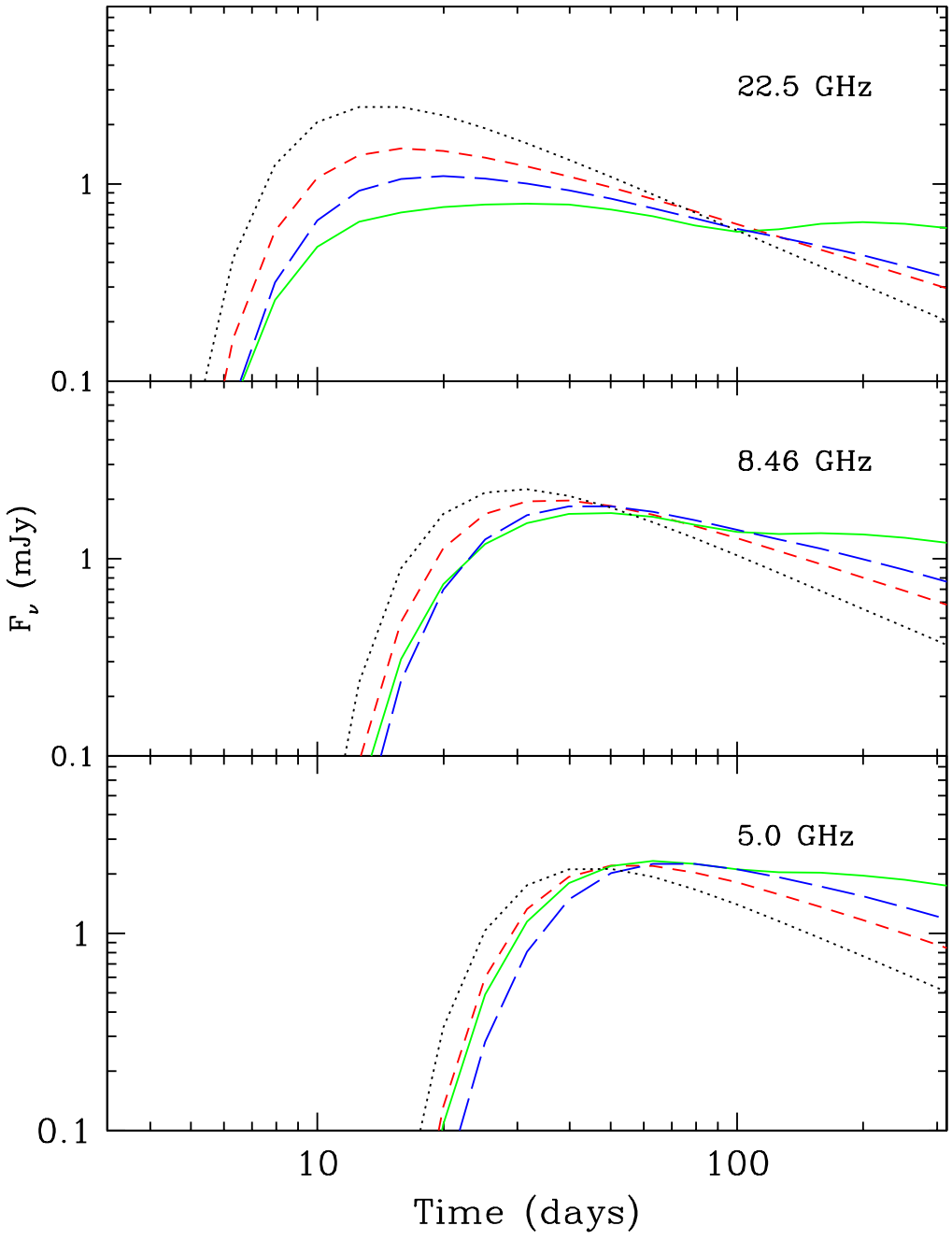

Fig. 4.— Radio light curves of four models with different cooling properties. The dotted line corresponds to a purely adiabatic model, the short dashed to a 'minimal cooling' model, the long-dashed curves to a model dominated by synchrotron cooling, and the solid curves to a model dominated by Compton cooling. See text for the parameters of each model.

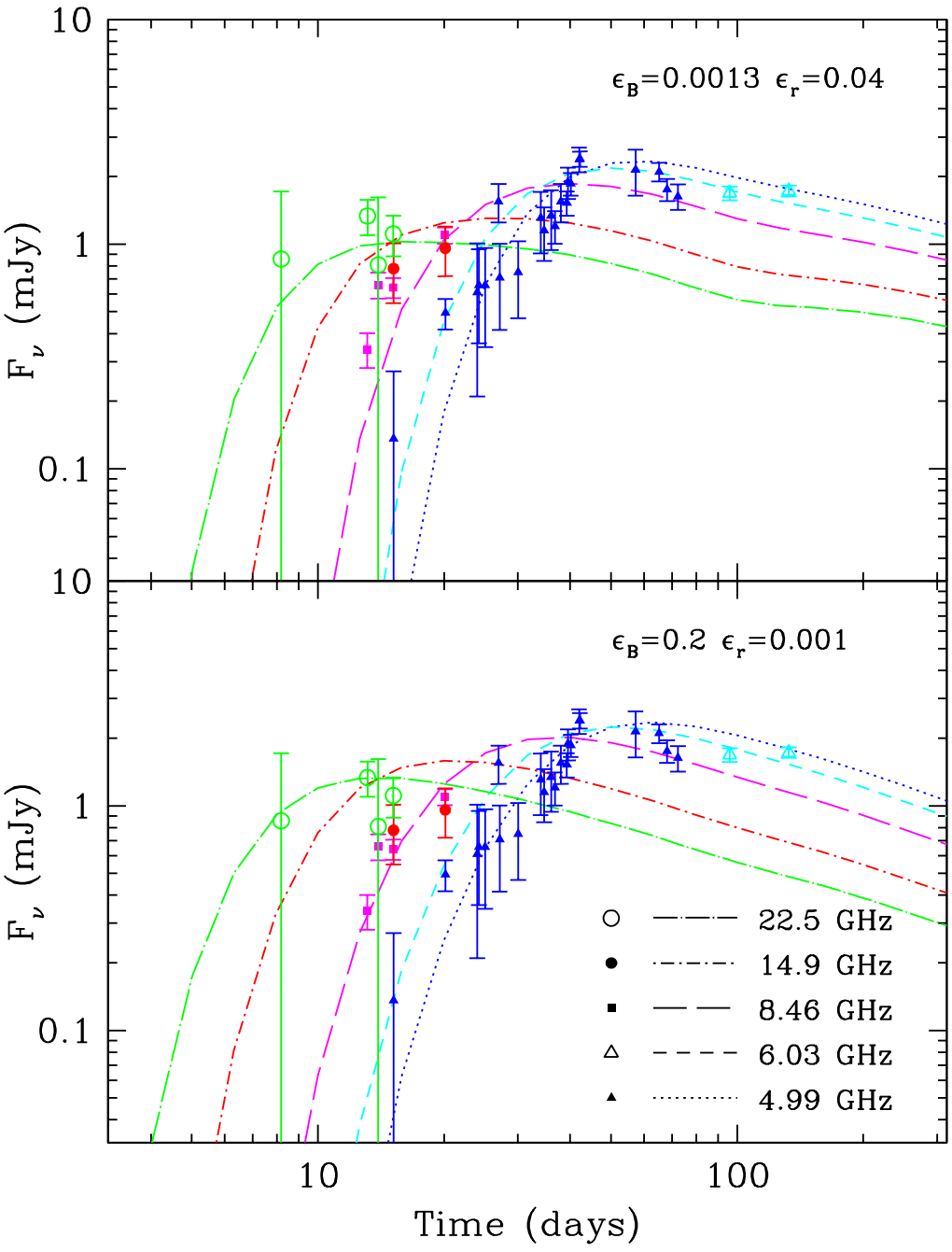

Fig. 5.— Observed radio light curves for SN 2004et compared to models with two different combinations of ϵ_B and ϵ_r. Note especially the effects of Compton cooling for the upper panel, resulting in nearly flat optically thin light curves, as well as the dip at $\sim$ 100 days seen at the high frequencies.

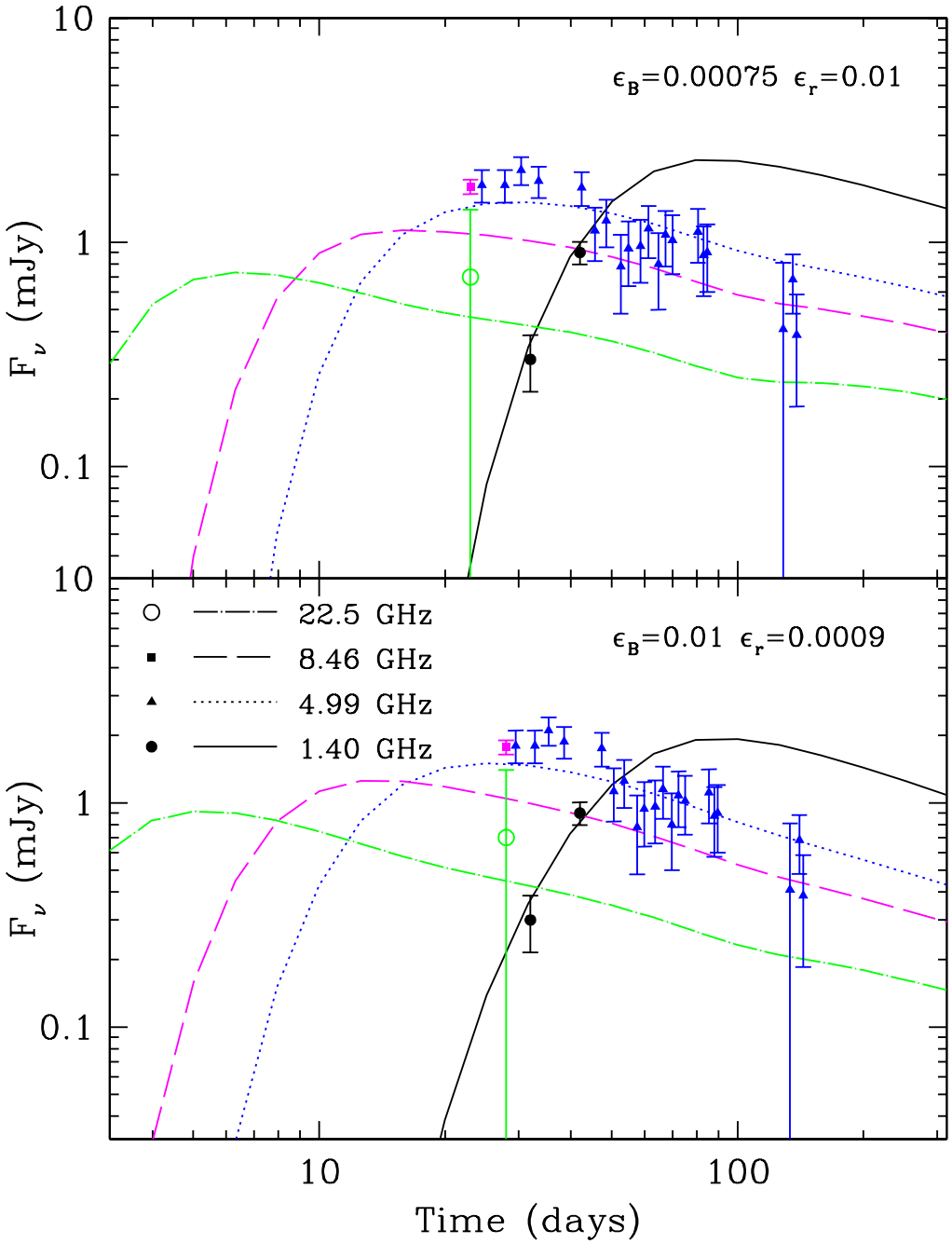

Fig. 6.— Observed radio light curves for SN 2004dj compared to models with two different combinations of ϵ_B and ϵ_r.

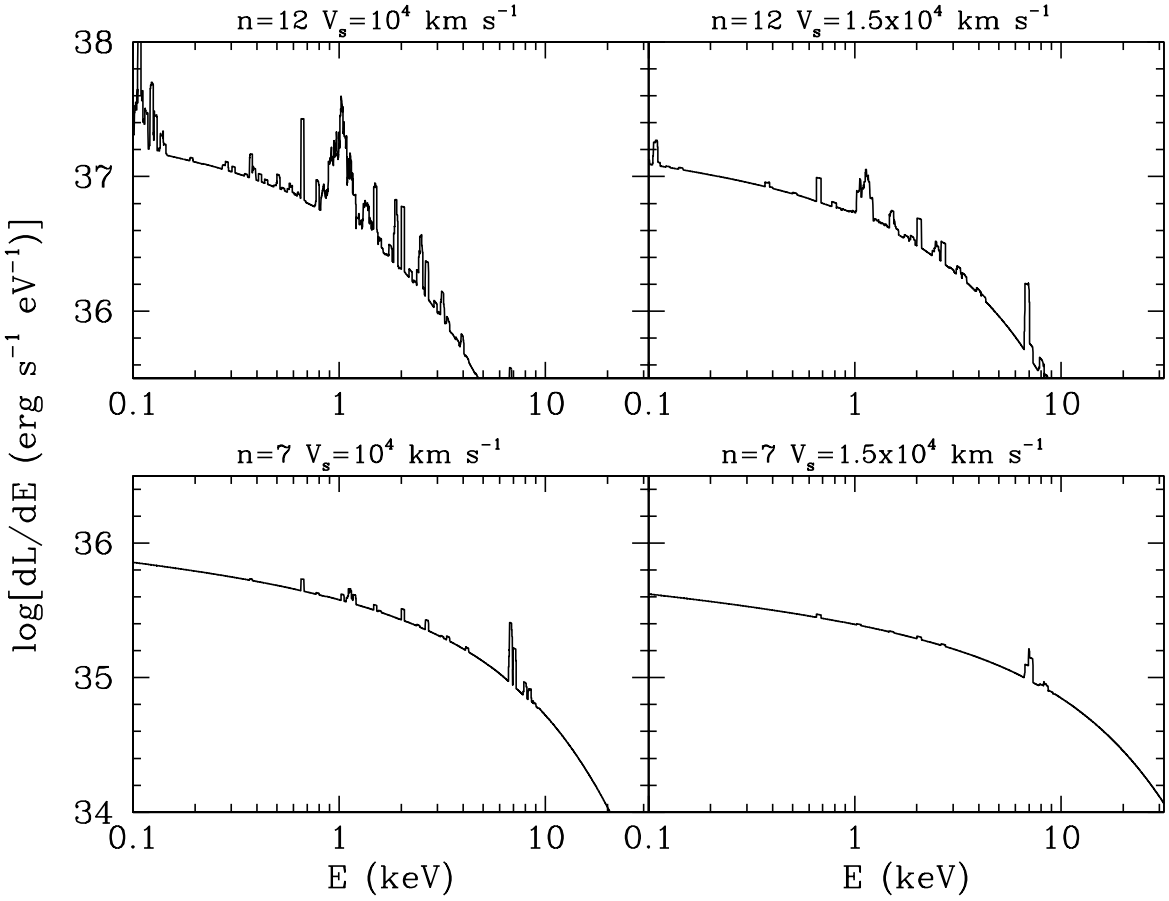

Fig. 7.— Calculated X-ray spectra for $n = 7$ and 12, and $V_s = 10,000$ km s^{-1} and $V_s = 15,000$ km s^{-1}. The mass loss rate is 5×10^{-6} $M_\odot$ yr^{-1} (for $v_w = 10$ km s^{-1}). Note the increasing importance of line emission as the reverse shock temperature decreases. For the highest temperature ($n = 7$ and $V_s = 15,000$ km s^{-1}) the only important lines are the Fe K lines at ~ 7.0 keV.